Hybrid and biocompatible cellulose/polyurethane nanocomposites with water-activated shape memory properties

Leire Urbina[a], Ana Alonso-Varona[b], Ainara Saralegi[a], Teodoro Palomares[b], Arantxa Eceiza[a], María Ángeles Corcuera[a,*], Aloña Retegi[a,*]

[a]'Materials + Technology' Group, Engineering School of Gipuzkoa. Department of Chemical and Environmental Engineering, University of the Basque Country (UPV/EHU), Pza. Europa 1., 20018 Donostia - San Sebastián, Spain

[b]Department of Cellular Biology and Histology, Faculty of Medicine and Odontology, University of the Basque Country (UPV/EHU), B. Sarriena, s/n 48940, Leioa-Bizkaia, Spain

Abstract

Water-activated shape memory bacterial cellulose/polyurethane nanocomposites were prepared by the immersion of bacterial cellulose (BC) wet membranes into waterborne polyurethane (WBPU) dispersions for different times. The high affinity between the hydrophilic BC and water stable polyurethane led to the coating and embedding of the BC membrane into the WBPU, facts that were confirmed by FTIR, SEM and mechanical testing of the nanocomposites. The mechanical performance of the nanocomposites resulted enhanced with respect to the neat WBPU, confirming the reinforcing effect of the BC membrane. An improvement of the shape fixity ability and faster recovery process with the presence of BC was observed. In 3 min, the nanocomposite with highest BC content recovered the 92.8 ± 6.3% of the original shape, while the neat WBPU only recovered the 33.4 ± 9.6%. The obtained results indicated that 5 min of impregnation time was enough to obtain nanocomposites with improved mechanical performance and fast shape recovery for potential biomedical applications. The present work provides an approach for developing environmentally friendly and biocompatible BC/polyurethane based materials with enhanced mechanical and shape memory properties.

Keywords: Bacterial cellulose; Waterborne polyurethane; Nancomposite; Biocompatible; Water-activated; Shape memory

1. INTRODUCTION

The technological developments that improve our health and life quality are based on the research and design of new materials with unique and improved properties. In recent years, smart materials with the ability to recover their original shape after being deformed in a temporary shape under the application of external stimulus, such as temperature, water, pH, light, etc, known as shape memory polymers (SMPs), have gained special attention (Hager, Bode, Weber,

& Schubert, 2015). Polyurethane (PU)-based thermoplastic polymers posses shape memory properties based on transition temperatures (glass transition or melting temperature) and also can be thermo-moisture responsive, since the moisture absorbed upon immersing into water has a strong influence on their properties (Sun & Huang, 2010). This means that these materials can be activated upon immersing into water. This interesting feature opens new possibilities for the application of PU and their nanocomposites in the biomedical field for the development of implants, drug delivery carriers, vascular stents, etc. allowing to minimizing invasive surgeries (Small, Singhal, Wilson, & Maitland, 2010). For example, SMP-PUs have been developed able to self-tight in a wireless manner (knot and suture) by immersing into water at room temperature. In addition, SMP-PU-based self retractable stents could be developed with the ability to expand in order to deliver a catheter and then, shrink back into original shape by water at room temperature to be removed easier (Huang, Yang, Zhao, & Ding, 2010).

Among PUs, the development of waterborne polyurethanes (WBPU) has experienced an increase because their use does not imply the use of organic solvents, thus reducing the amount of volatile organic compounds released to the atmosphere (Zhou et al., 2015). Moreover, WBPU dispersions present low viscosities and good film forming ability with strong adhesion and large flexibility which make them interesting for the development of different nanocomposites (Wan & Chen, 2018; Zhang, Xu, Fan, Sun, & Wen, 2019). In addition, these matrixes in aqueous dispersion present good affinity with hydrophilic nanoentities and nanoreinforcements, such as polysaccharides derivatives, which leads to an improvement of the thermo-physical and mechanical properties of the resulting polyurethanes (Santamaria-Echart et al., 2016; Wang et al., 2019). Among polysaccharides, nanocellulosic materials have gained much attention due to their numerous potential applications in nanotechnology (Jiang et al., 2018; Thomas et al., 2018). Nanocellulose is widely used as a nanoentity for preparation of advanced nanostructured materials, since the use of nanocelluloses as reinforcements leads to an enhancement of some properties, especially, mechanical properties. However, in order to obtain advanced nanocomposites, a proper dispersion of the nanoentity in the matrix must be achieved. Nanocelluloses possess active hydroxyl groups which can interact by hydrogen bonding with the macromolecular chains of WBPU matrixes leading to an increased dispersion, reinforcement and interfacial adhesion (Solanki, Das, & Thakore, 2018). Furthermore, nanocellulose can be considered a good substrate material for water-activated shape memory materials due to its surface´s hydroxyl groups and intermolecular hydrogen bonds. Song et al., 2018 developed a cellulose based water-activated shape memory composite with sisal cellulose nanofibers and graphene oxide which reached a shape recovery ratio nearly of 100%.

In this way, bacterial cellulose which is produced by some bacterial strains in the form of a gelatinous and translucent membrane, has an interesting 3D nanofiber network conformation.

This spatial configuration favours the inter-chain hydrogen bonds generating a tight and strong cellulose nanofiber network with high mechanical properties and stability even in moist environments. This feature makes BC an interesting template for the development of a wide range of nanocomposites (Hu, Chen, Yang, Li, & Wang, 2014). In addition the use of BC membrane as a nanoreinforcement could be an interesting possibility to counteract the difficulty to obtain a good dispersion of the nanoentities in polymer matrixes. In fact, BC has been used in the preparation of nanocomposites with PUs and PU prepolymers based on castor oil showing good adhesion, transparency and flexibility with potential applications in electronic devices (Pinto, Barud, Polito, Ribeiro, & Messaddeq, 2013, 2015). Moreover, due to its biocompatibility, BC exhibits interesting properties for in vivo and in vitro applications in biomedicine (Picheth et al., 2017). Wu et al. (2014) developed silver nanoparticle/BC hybrid gel-membranes with improved antimicrobial activity to use them as an antimicrobial wound dressing. Kim, Cai, and Chem, (2010) developed BC/chitosan, BC/polyethylene glycol and BC/gelatine composites for tissue-engineering scaffolds and wound dressing materials by the immersion of BC pellicles in the polymeric solutions.

In the present work, water-activated nanocomposites based on WBPU and BC have been developed. The use of water-dispersed polyurethanes facilitates the preparation of nanocomposites without the use of organic solvents and solvent exchanges for the BC membranes which have strong affinity with water. There are other works in which nanocelluloses (El-Fattah, Hasan, Keshawy, El Saeed, & Aboelenien, 2018), cellulose nanocrystals (Santamaria-Echart et al., 2016) or bacterial cellulose (Pinto et al., 2013, 2015) have been used to prepare composites with polyurethanes. However, to the best of our knowledge, no work has been found which exploits the potential of the whole BC membrane as a template for waterborne polyurethanes to prepare nanocomposites with proven enhanced water-activated shape memory properties and biocompatibility. For this, BC membranes have been embedded into WBPU dispersion to produce nanocomposites with improved stiffness and enhanced shape memory properties. The morphology, interactions between polymers and thermal, thermomechanical and mechanical properties of the nanocomposites have been investigated by scanning electron microscopy (SEM), Fourier transform infrared spectroscopy (FTIR), thermogravimetric analysis (TGA), differential scanning calorimetry (DSC), dynamic-mechanical analysis (DMA) and tensile tests. In order to evaluate the potential applications of these nanocomposites in the biomedical field, the in vitro biocompatibility was studied by cytotoxicity and cell adhesion assays. Additionally, water-activated shape memory properties were analysed by fold-deploy shape memory test method. The results obtained prove that high performance water-activated shape memory nanocomposites can be developed for biomedical applications using two

biocompatible and eco-friendly materials, WBPU dispersion and BC membranes, following an easy impregnation method.

2. MATERIALS AND METHODS

2.1. Chemicals

Bacterial cellulose culture medium was prepared with apple residues collected from a cider producer of Gipuzkoa (Northen Spain) and commercial sugar cane. Potassium hydroxide (KOH) and acetic acid glacial (technical grade) were obtained by Panreac Applychem. Impraperm DL 3746 WBPU with 37 wt% of solids content and 87.1 ± 0.3 nm particle size and 0.083 ± 0.016 polydispersity (determined by light scattering) was kindly supplied by Covestro (Germany). N,N-dimethylformamide (DMF) was purchased from Aldrich. Phosphate buffered solution (PBS) and calcein-AM were supplied by Sigma-Aldrich (St Louis, MO, EEUU). Sodium pyruvate and non-essential amino acids were obtained by Gibco (Life Technologies, UK). Penicillin-streptomycin was supplied by Lonza (Sweden) and fetal bovine serum by Biochrom AG (UK). Ethidium homodimer-1 was supplied by Molecular Probes (Eugene, Oregon, USA).

2.2. Preparation of BC/WBPU nanocomposites

Firstly, BC membranes were grown in a culture medium prepared with a mixture of apple residues from the cider production and sugar cane according to a published protocol (Urbina et al., 2017). Then, BC membranes were purified by treating with KOH solution (2 wt%) for 24 h at room temperature, in order to remove non-cellulosic compounds, and thoroughly washed with running water until a complete neutralization. BC/polyurethane nanocomposites were prepared by immersing BC wet membranes in 50 mL of the commercial WBPU dispersion under stirring conditions at room temperature for different times, 5, 30, 60 and 120 min. Subsequently, the membranes were removed from the dispersion and drained. Finally, these were dried at room temperature for 4 days in order to obtain transparent nanocomposite films. The as prepared nanocomposites were designated as BC/WBPU5, BC/WBPU30, BC/WBPU60 and BC/WBPU120, where the number indicates the immersion time. As a reference, a neat WBPU film was prepared by casting and dried in the same conditions as the nanocomposites. Additionally, neat BC films were prepared by drying the BC membranes between Teflon plates to avoid the shrinkage in the oven at 55 °C for two days. In the case of the BC/WBPU nanocomposites, the drying method followed for the neat BC membranes was not be suitable because this PU presented a transition temperature around 50 °C, so a slow drying process at room temperature was preferable. The thickness of the nanocomposites, neat WBPU film and neat BC membrane in dry state was measured with a gauge.

2.3. Characterization of BC/WBPU nanocomposites

In order to estimate the composition of the nanocomposites, the amount of BC was determined in the BC/WBPU5 and BC/WBPU120 nanocomposites, which were the membranes prepared with the shortest and the largest immersion times. For this, consecutive extractions with DMF, which resulted to be an effective solvent for PU removal, were carried out for a week to ensure the complete removal of the PU from the BC membrane. This fact was confirmed by FTIR analysis of the resultant dried BC samples, as no characteristic bands corresponding to the PU were observed in the FTIR spectra of the dried samples. Finally, DMF was eliminated from the extract in a rotary evaporator (100 mbar, 97 °C). The amount of BC in the nanocomposites was estimated using two variables: through the weight difference between the initial nanocomposite and the BC after the elimination of PU, and though the weight difference between the WBPU/DMF and the collected WBPU after DMF removal from the flask. Each system was measured in duplicate. All the samples were kept in a desiccator in order to avoid humidity effects before each characterization procedure.

SEM was used to analyze the cross sections of the neat BC and BC/WBPU5 nanocomposite. Prior to SEM assay, films were freeze-fractured with liquid nitrogen in order to expose the cross section of the film. Scanning electron microscope JEOL JSM-6400 was used with a wolframium filament operating at an accelerated voltage of 20 kV and at a working distance of 5–10 mm. Samples were coated with approximately 20 nm of chromium using a Quorum Q150 TES metallizer.

FTIR spectroscopy was used to analyze the possible interactions between BC and WBPU in the nanocomposites. A Nicolet Nexus spectrophotometer provided with MKII Golden Gate accessory (Specac) with diamond crystal at a nominal incidence angle of 45° and ZnSe lens was used. Spectra were recorded in attenuated total reflectance (ATR) mode between 4000 and 650 cm^{-1} averaging 32 scans with a resolution of 4 cm^{-1}.

Mechanical testing was carried out at room temperature using an Universal Testing Machine (MTS Insight 10) with a load cell of 10 kN and pneumatic grips. Samples were cut in 30×5 mm^2 rectangular specimens. For the determination of the elastic modulus (E), a crosshead rate of 0.5mm min^{-1} was set using a video extensometer. Maximum strength (σ_{max}) and elongation at break (ε_b) were measured at a crosshead rate of 50mm min^{-1} using also a video extensometer. At least seven samples were tested for each set of samples, being the average values reported.

Thermal properties were studied by DSC using a Mettler Toledo 822e equipment, provided with a robotic arm and an electric intracooler as the refrigerator unit. Aluminium pan containing sample (5–10 mg) was heated from -75 to 200 °C at a scanning rate of 2 °C min^{-1} in nitrogen atmosphere. Glass transition temperature was determined as the inflection point of the heat capacity change, whereas melting temperature and enthalpy were established as the maximum and the area under the endotherm peak, respectively.

Thermal degradation was studied by TGA. Measurements were performed by using a TGA/SDTA 851 Mettler Toledo instrument. Samples (2 mg) were scanned from 25 to 800 °C at a heating rate of 10 °C min^{-1}. These tests were carried out under nitrogen atmosphere in order to prevent the thermoxidative degradation.

Thermomechanical behavior was analyzed by DMA using an Eplexor 100 N analyser, Gabo equipment. Tensile mode measurements were carried out from -100 to 100 °C at a scanning rate of 2 °C min^{-1}. The static strain was established as 0.05% and the operating frequency was fixed at 1 Hz.

For the swelling study of the neat WBPU and BC/WBPU nanocomposites, three samples of each one were immersed in deionized water during 24 h at room temperature. At different time intervals, samples were removed from water, wiped with filter paper for free water removal and then weighed. The water holding capacity (WHC) was calculated from Eq. 1:

$$WHC\ (\%) = \left(\frac{W_{wet} - W_{dry}}{W_{dry}}\right) \cdot 100 \qquad (1)$$

where W_{wet} is the weight of swollen samples at different times and W_{dry} is the weight of the previously dried samples.

2.4. Biocompatibility tests

The in vitro biocompatibility of the neat BC membrane and the nanocomposite prepared with the shortest immersion time (BC/WBPU5 nanocomposite) was confirmed by cytotoxicity assay as well as adhesion tests (cell viability (Live/Dead)).

Short-term cytotoxicity tests with neat BC and BC/WBPU nanocomposite were performed in order to evaluate the presence and/or release of toxic degradation products. The extractive method ISO 10993−11:2009 was used. Cytotoxicity was assessed by PrestoBlue® (Invitrogen, USA), a resazurin-based solution that functions as a colorimetric cell viability indicator. For this assay, murine fibroblasts (L929 cells) were seeded into 96-well plates at a density of 4×10^3 cells/well in 100 µL of complete culture medium. After 24 h, the medium was replaced with 100 µL of negative control (complete medium), positive control (DMSO, 10% in complete medium) or biomaterial´s extractive media and a 10% of PrestoBlue® was added. The optical density was measured at 570 and 600 nm in a spectrophotometer (Synergy HT spectrophotometer, Biotek, USA) at different time points (0, 24 and 48 h). The viability of the cells was calculated following the Eq.2.

$$Viability\ (\%) = \frac{[Abs]_{sample}}{[Abs]_{negative\ control}} \cdot 100 \qquad (2)$$

where $[Abs]_{sample}$ is the absorbance of the sample cells and $[Abs]_{negative\ control}$ is the absorbance of the negative control cells (in this case highdensity polyethylene). All assays were conducted in triplicate and average values and standard deviations were estimated.

The analysis of cell long term adhesion was carried out by performing Live/Dead assays. Samples of 0.5 cm^2 were prepared (3 replicates for each sample) and prior to analysis the materials were sterilized. Neat BC was sterilized with ethanol 70% (v/v) for 2 h, while BC/WBPU nanocomposite was sterilized under ultraviolet light for 30 min (to prevent the dissolution of the WBPU). Then, materials were washed 3 times with phosphate buffered saline (PBS from Sigma-Aldrich) and incubated in 500 μL of a complete medium (Dulbecco's modified Eagle's medium (DMEM) supplemented with sodium pyruvate 1 mM, 1% of non-essential amino acids, 1% penicillin-streptomycin and fetal bovine serum 10%) at 37 °C for 24 h. After pre-wetting, the medium was removed and 50,000 cells (Murine fibroblasts L929) were seeded on the materials according to ISO 10,993-11: 2009. After incubating for 90 min to ensure adhesion, PBS was added to the surrounding wells to prevent drying. Finally, 500 μL of complete medium was added to the wells with materials. Images of the samples were taken after 3, 7 and 14 days. The medium was removed and samples were washed with PBS three times. Subsequently, calcein-AM 4mM and ethidium homodimer-1 in PBS were added. Calcein-AM ($\lambda_{ex}/\lambda_{em}$: 495/515 nm) reports the esterase activity of living cells emitting in green and homodimer-1 emits in red ($\lambda_{ex}/\lambda_{em}$: 493/630 nm), indicating the loss of integrity of the plasma membrane (Althouse & Hopkins, 1995). After incubating the samples in the dark at 37 °C for 20 min, the analysis was carried out in an Olympus LV500 confocal microscope (Olympus, Japan).

2.5. Shape memory behaviour

The shape memory effect was investigated by fold-deploy shape memory test (Cai, Jiang, Zheng, & Xie, 2013; Liu, Han, Tan, & Du, 2010). Samples (30×10mm^2) were immersed in a water bath at 60 °C inside closed containers and folded (θ_d) by applying external constant force. Then, they were cooled down in an ice water bath under the external force to fix the temporary shape. This force was then removed after holding for several minutes and a marginal recovery occurred (θ1) and the bending angle became fixed (θ_f). Finally, the specimens were immersed in water at 40 °C and the change of the angle with time (θ_t) was recorded using a video camera. The shape fixity ratio (R_f) and the shape recovery ratio (R_r) were calculated from Eqs. 3 and 4, respectively.

$$R_f = \frac{\theta_f}{180^\circ} \cdot 100 = \frac{180^\circ - \theta_1}{180^\circ} \cdot 100 \quad (3)$$

$$R_r = \frac{\theta_t - \theta_1}{180^\circ - \theta_1} \cdot 100 \quad (4)$$

The measure of the bending test angles was carried out through an open source image-processing program, ImageJ. Each system was tested in triplicate in order to calculate the standard deviation. The shapememory study procedure is indicated in **Scheme 1**, where the temperatures of each phase are presented: T_s (storage temperature), T_d (deformation temperature), T_f (fixation temperature) and T_r (recovery temperature).

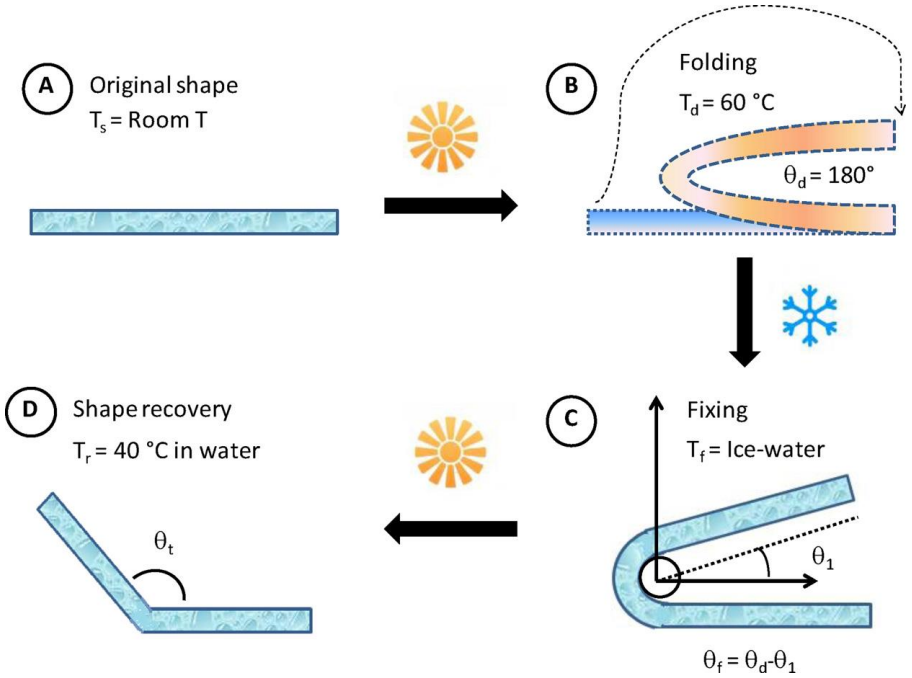

Scheme 1. Fold-deploy shape memory test procedure.

3. RESULTS AND DISCUSSION

3.1. Characterization of BC/WBPU nanocomposites

Firstly, the effect of the impregnation time of the WBPU dispersion into BC membranes in the morphology and thickness of the resulting BC/WBPU nanocomposites was analyzed. As it can be observed in Table 1, there is a direct relationship between the impregnation time and the thickness of the nanocomposites. As the impregnation time increased, the thickness of the nanocomposite was greater, which suggests that the quantity of WBPU in the BC/WBPU nanocomposite was higher.

It was estimated that BC/WBPU5 contained a 1.8 ± 0.1 wt% of BC while BC/WBPU120 contained 0.6 ± 0.1 wt% of BC (data obtained by the weight difference between the initial nanocomposite and the BC membrane after the elimination of PU, although the results obtained with both methodologies were very similar). These results confirmed that the nanocomposites contained high amount of polyurethane, probably due to the high affinity between both polymers and the BC porous structure. In this way, the porous structure of the BC nanofiber network and the nanometric size of WBPU particles (87.1 ± 0.3 nm) in water probably favoured the penetration

and coating of the BC structure. Additionally, the polyurethane used in this work was water based, which probably facilitated the diffusion and impregnation of the WBPU nanoparticles into the BC wet membrane as both components were hydrophilic. Some preliminary experiments were performed with dry BC membranes and the results confirmed that the impregnation was more effective in the case of using wet membranes. This was probably due to the fact that BC membranes were already swollen, which led to a greater diffusion of the WBPU nanoparticles though the BC membranes at the studied time intervals.

Table 1. Thickness of neat BC membrane, BC/WBPU nanocomposites and neat WBPU.

Sample	Thickness (mm)
BC	0.04 ± 0.01
BC/WBPU5	0.22 ± 0.05
BC/WBPU30	0.33 ± 0.05
BC/WBPU60	0.35 ± 0.07
BC/WBPU120	0.42 ± 0.05
WBPU	0.43 ± 0.17

This fact was confirmed by SEM analysis. Fig. 1 a), b) and c) shows the microstructure of the cross section of the BC membrane (x10,000, x250 and x1,000, respectively). In Fig. 1 e) and f) the microstructure of the cross section of BC/WBPU5 nanocomposite can be observed (x250 and x1,000). As it can be seen, BC presented the typical compacted layered structure with nanofibrous conformation (Bodin et al., 2006; Klemm, Schumann, Udhardt, & Marsch, 2001). In the case of the nanocomposite, the presence of the BC was not appreciated due to the high amount of WBPU and the embedding of the BC membrane into the WBPU. This fact, resulted in an increase of film thickness and made it very complicated to observe the BC into the nanocomposites by SEM.

As it can be observed in Fig. 1. d), BC/WBPU nanocomposites exhibited excellent transparency. It has been previously reported that the nanofiber papers are translucent due to the effect of the light diffraction at the interface between the cellulose nanofibers and the air interstices between them (Nogi, Iwamoto, Nakagaito, & Yano, 2009). The 3D nano-sized fiber network of the BC with air interstices in between makes it very translucent, so the transparency of the nanocomposites implies that these gaps may had been completely filled by the polyurethane and the surface had been coated. This was also observed in a previous work developed in our research group in which BC membranes were impregnated with poly(lactic acid) (PLA), although the effect was less pronounced as PLA and BC did not show such a good affinity (Urbina et al., 2016). These results would confirm that as the polyurethane used in the present work was water based,

it presented strong affinity with BC which contains numerous OH groups in its chemical structure, leading to nanocomposites with high amount of the last.

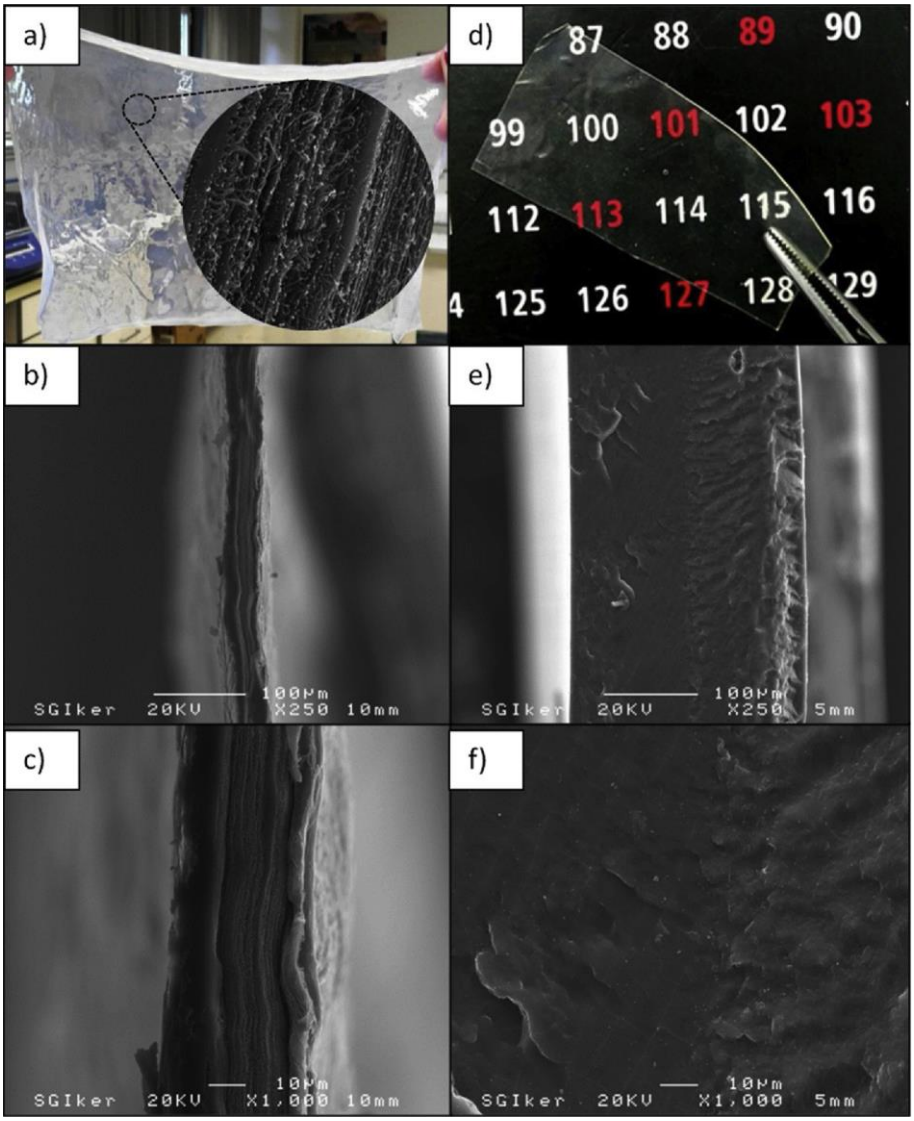

Fig. 1. a) BC wet membrane and SEM image of the cross section x10,000, b) and c) SEM images of cross section of BC membrane (x250, and x1,000, respectively), d) BC/WBPU5 transparent nanocomposite, e) and f) SEM images of cross section of BC/WBPU5 nanocomposite (x250 and x1,000, respectively).

To identify the possible interactions between BC and WBPU in the nanocomposites, FTIR spectroscopy analysis was carried out. In Fig. 2. a), the FTIR spectra of neat BC, neat WBPU and BC/WBPU5 are shown (FTIR spectra of the other nanocomposites were almost identical to the one presented). The neat WBPU showed the typical bands of the repetitive urethane group (-$NHCOO^-$). The band located at 3440 cm^{-1} corresponds to stretching vibration of N–H bond and the band at 1530 cm^{-1} is assigned to the in-plane bending vibration of N–H. The bands at 2920 and 2850 cm^{-1} are associated to stretching vibration of C–H. The characteristic band about 1730 cm^{-1} is related with the urethane C=O group. The band at 1259 cm^{-1} corresponds to asymmetric

stretching vibration of C–O (Jiao, Xiao, Wang, & Sun, 2013; Santamaria-Echart et al., 2016). In the case of BC membrane, the broad band around 3340 cm^{-1} corresponds to O–H cellulose stretching vibrations. The absorption bands at 2900−2880 and 1430 cm^{-1} are assigned to the CH and CH_2 stretching and bending vibrations, respectively. The C–O–C bond of the glycosidic bridges corresponds to the bands at 1160 and 1108 cm^{-1}, while the band at 898 cm^{-1} is characteristic of β-linked glucose based polymers (Urbina et al., 2017). The band at 1646 cm^{-1} is associated with the water absorbed by the cellulose. In the nanocomposite spectrum, the peaks of the BC are not observed due to the high content and coating of WBPU. The FTIR spectra of the neat WBPU and the nanocomposite were very similar, therefore a second-derivative spectroscopy analysis was used to ascertain if differences between them could be observed. The second-derivative spectra in the range of 1500−900 cm^{-1} were almost identical for the two samples, as it can be observed in Fig. 2. b). However, significant differences were found in the OH stretching vibration region in the range 3500−3290 cm^{-1} as showed in Fig. 2. c), where it can be clearly seen a shift in the bands at 3495, 3486, 3421, 3411, 3338, 3320 and 3301 cm^{-1} in the case of the nanocomposite. Guo, Sato, Hashimoto, and Ozaki, (2010) analyzed the hydrogen bonding interactions of poly (3-hydroxybutyrate) and poly(4-vinylphenol) blends through the second derivative spectra. They observed bands in this region which were shifted in the case of the blend to higher wavenumbers with respect to the neat components and they attributed the shifting of these bands to intermolecular hydrogen bonding. In this case, the results indicate that hydrogen bonding interactions between BC and WBPU have been formed in the nanocomposite.

The mechanical behavior of neat BC, WBPU, and BC/WBPU nanocomposites was evaluated by tensile tests and their maximum strength (σ_{max}), elastic modulus (E), and elongation at break (ε_b) obtained from stress-strain curves are gathered in Table 2. BC exhibits an outstanding high modulus due to the conformation of the 3D structure of the interconnected nanofibrils formed during the its biosynthesis (Feng et al., 2015; Nakagaito, Iwamoto, & Yano, 2005). The high content of WBPU in the nanocomposites is evident taking into account the results obtained in the mechanical properties. The commercial WBPU used in this work exhibits a remarkable elastomeric behavior and the prepared BC/WBPU nanocomposites present also a high elongation at break. It is observed a decline in elongation at break of the nanocomposites with shorter impregnation times due to the higher content of BC, although still maintained the elasticity of the WBPU (ε_b values superior than 400% in all nanocomposites). In addition, the strength and modulus of the nanocomposites experienced an improvement with respect to the neat WBPU, suggesting the reinforcing effect of the BC membrane. An improvement of 26% and 10% in tensile strength was observed compared to the neat WBPU for the BC/WBPU5 (~1.8 wt% BC) and BC/WBPU120 (~0.6 wt% BC), respectively. In the same way, the elastic modulus experienced an increase of 475% and 110% compared to the neat WBPU for the BC/WBPU5 and

BC/WBPU120, respectively. In this work, this fact could be due to the good interfacial interactions between both polymers as it has been observed by other authors (Alemi & Shodja, 2018). Wu, Liu, Chen, and Kong, (2017) prepared nancomposite films from a two-component waterborne polyurethane with 0.5, 1, 1.5, and 2 wt% contents of nanofibrillated cellulose (NFC). They observed enhancement in the modulus and tensile strength up to 1% of nanofiller with respect to the neat polyurethane ascribed to the uniform dispersion and interfacial bonding of the NCF with the polyurethane. However, the increase of the NFC content led to a decline of the mechanical performance, attributed to the self aggregation of NFC. As expected, elongation at break of the nanocomposite films decreased with the increase of NFC content. In the present work, the randomly oriented nanofiber membrane of BC is completely embedded in the WBPU and the use of the whole BC membrane counteracts the difficulties to obtain a better dispersion of nanofibers. In addition, these results would be in accordance to the ones obtained in the FTIR analysis, where interactions between BC and polyurethane have been observed. In view of these results, 5 min of impregnation would be enough time to obtain stiffer yet deformable nanocomposites with high content of WBPU.

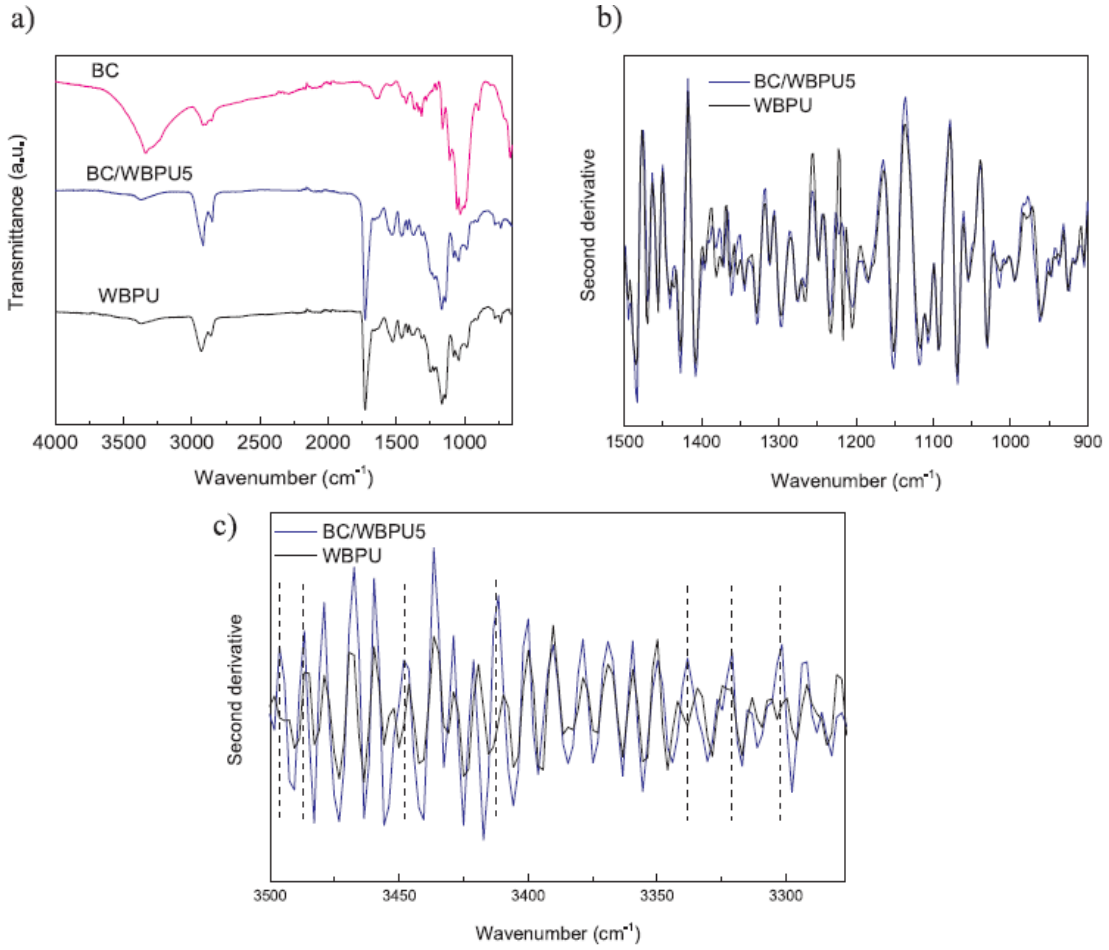

Fig. 2. a) FTIR spectra of the neat BC, neat WBPU and BC/WBPU5 nanocomposite, and second derivative curves of neat WBPU and BC/WBPU5 nanocomposite b) between 1500−900 cm^{-1} and c) between 3500−3290 cm^{-1}.

Additionally, the thermal and thermomechanical properties of BC/WBPU nanocomposites were analyzed. For these studies BC/WBPU5 and BC/WBPU120 were chosen since these are the nanocomposites with higher and lower content of BC, and the results were compared to those obtained for the neat BC and neat WBPU.

Table 2. Mechanical properties of neat BC membrane, BC/WBPU nanocomposites and neat WBPU.

Sample	E (MPa)	σ_{max} (MPa)	ε_b (%)
BC	7120.3 ± 421.3	116.9 ± 17.0	2.5 ± 0.3
BC/WBPU5	41.4 ± 5.1	11.6 ± 2.9	464.3 ± 31.8
BC/WBPU30	28.7 ± 3.5	9.7 ± 1.7	582.8 ± 76.0
BC/WBPU60	25.1 ± 3.8	10.3 ± 2.7	711.5 ± 77.1
BC/WBPU120	15.2 ± 2.8	10.1 ± 1.4	697.3 ± 68.7
WBPU	7.2 ± 1.7	9.2 ± 2.5	917.7 ± 96.4

Thermal transitions of neat BC, neat WBPU and BC/WBPU nanocomposites were analyzed by differential scanning calorimetry and the obtained thermograms are shown in Fig. 3. a). In the case of neat BC, a weak endothermic transition was observed in the temperature range of 35–120 °C. This can be ascribed to the dehydration process of cellulose (Ciolacu, Ciolacu, & Popa, 2010). Regarding the WBPU and the nanocomposites, the presence of two transitions was observed. The one at low temperature (from -70 to -40 °C) was related with glass transition (T_g) of the soft segment of WBPU and the second one at higher temperature (in the range of 50–120 °C), an endothermic peak, associated to melting process (T_m). The values of glass transition temperature (T_g), melting temperature (T_m) and melting enthalpy (ΔHm) are gathered in Table 3. No significant changes were observed in the case of T_g and T_m between WBPU and the nanocomposites. However, it can be noted that the melting enthalpy increased with BC content. BC/WBPU5 nanocomposite, which was the one with highest BC content, presented the highest melting enthalpy followed by the BC/WBPU120 nanocomposite and finally the neat WBPU. This suggested that the presence of BC in the WBPU may have induced a nucleating effect, favouring its crystallization (Auad, Contos, Nutt, Aranguren, & Marcovich, 2008).

In addition, thermal stability of neat BC, neat WBPU and BC/WBPU nanocomposites was studied by thermogravimetric analysis. Besides, this study was used to corroborate that the last transition observed in the range of 50–120 °C in the WBPU and BC/WBPU nanocomposites was not related to the evaporation process of possible water content present. The TG curves are shown in Fig. 3. b). In the case of neat BC, the first initial mass loss below 150 °C is usually associated to the release of water, while the volatilization of thermally degraded cellulosic compounds is in the range of 200–500 °C (Kiziltas, Kiziltas, & Gardner, 2015). As it can be observed, the neat WBPU

does not contain water, nor the BC/WBPU nanocomposites as no mass loss is observed up to temperatures around 300 °C. The presence of BC induces to an earlier degradation in the nanocomposites, since as it can be observed the corresponding TGA curves of the nanocomposites are shifted towards lower temperatures compared to the neat WBPU. The temperature at 10 and 50% of mass loss (T_{10} and T_{50}, respectively) are shown in Table 3, where it can be observed a decrease of around 10 °C in the case of the temperature at 10% mass loss of the nanocomposites with respect to the neat WBPU.

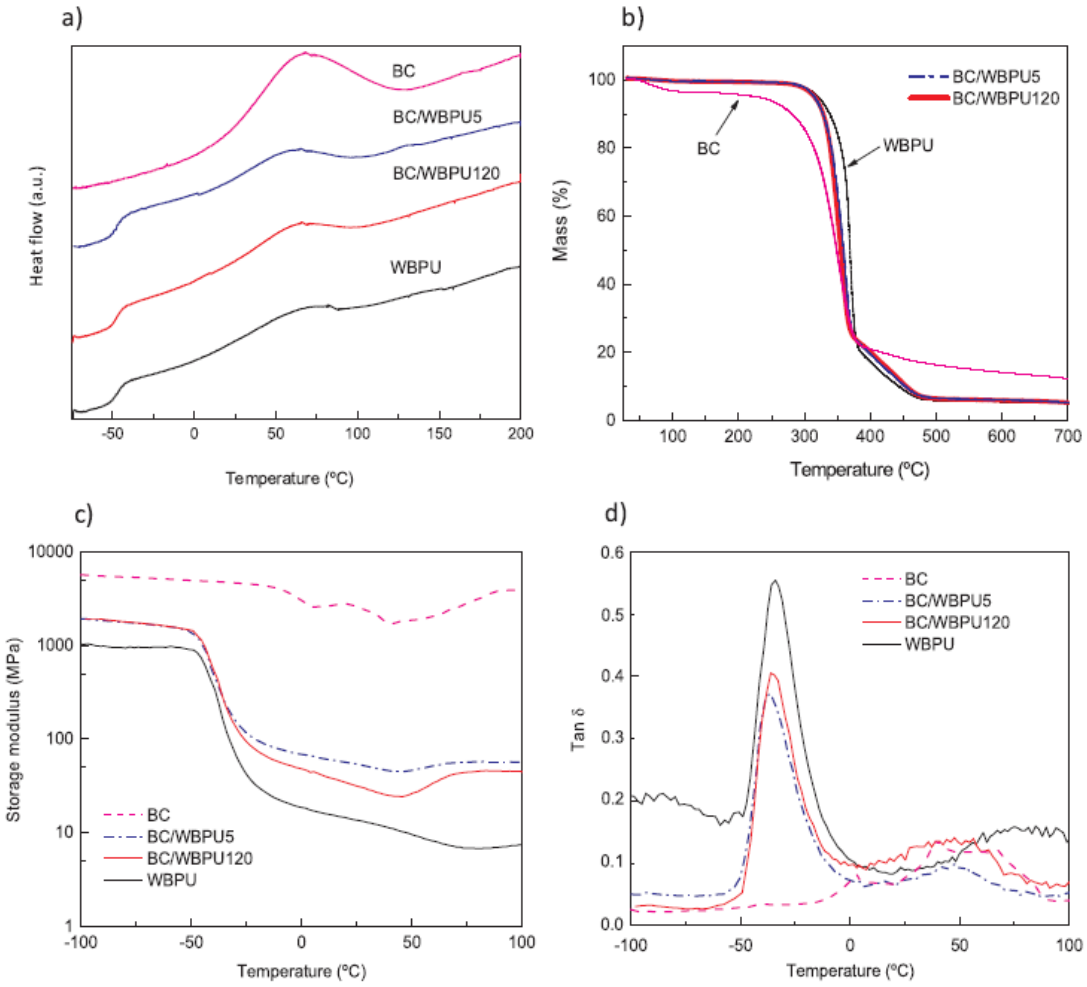

Fig. 3. a) DSC thermograms, b) TGA curves, c) Storage modulus and d) Tan δ of neat BC, neat WBPU, BC/WBPU5 and BC/WBPU120.

Finally, the thermomechanical behavior of the different samples was studied by dynamic-mechanical analysis. The evolution of storage modulus (E´) and Tan Delta (Tan δ) curves as a function of temperature are shown in Fig. 3. c) and d), respectively. In the case of the neat BC, a drop in the storage modulus and a maximum in the Tan δ in the range of -10 to 50 °C can be observed, associated to the presence of water into the structure that acts as plasticizer which was in agreement with the TGA. This behavior was also observed by other authors (Figueiredo et al., 2013). Compared to neat WBPU, both nanocomposites showed higher storage modulus (E') on

all temperature range. In the glassy state, at very low temperatures (from -100 to -40 °C), neat BC presented the highest E´ value (5700 MPa) while the neat WBPU presented the lowest value (1040 MPa) and, as it can be observed, BC/WBPU nanocomposites showed intermediate E´ values between neat components. Similar E´ values were observed for both nanocomposites, 1900 and 1920 MPa for BC/WBPU5 and BC/WBPU120, respectively. As the temperature increased, the storage modulus of the neat WBPU and both nanocomposites showed a significant decrease associated with the glass transition temperature. This tendency was the same as the one observed in the DSC. In the case of neat WBPU, the modulus kept decreasing with temperature in the rubbery region due to the thermoplastic nature of the material, while in the BC/WBPU nanocomposites the drop was not so pronounced due to the reinforcing effect of BC network into the WBPU. This effect was also observed by other authors in a polyurethane elastomer reinforced with 0.5, 1 and 5 wt% of cotton cellulose nanocrystals (Pei, Malho, Ruokolainen, Zhou, & Berglund, 2011). They ascribed this effect to the increase of the cross-linked density of the material through polyurethane-cellulose interactions. In the present work, a slightly increase of the modulus above 50 °C was observed in the case of the nanocomposites. Around the Tm of the WBPU, the polymer mobility could favour the formation of interactions between BC and WBPU, and therefore a slight increase in the modulus.

Table 3. Thermal properties of neat BC membrane, BC/WBPU nanocomposites and neat WBPU.

Sample	T_g (ºC)		T_m (ºC)	ΔH_m (J g^{-1})	T_{10} (ºC)	T_{50} (ºC)
BC	-	-	-	-	280	349
BC/WBPU5	-47.6*	-42.8**	63.9	19.9	325	354
BC/WBPU120	-46.6*	-43.7**	65.4	15.4	326	358
WBPU	-48.2*	-44.6**	64.2	12.3	335	370

T_g values measured by DSC (*) and DMA (**).

3.2. Biocompatibility: cytotoxicity assessment and cell adhesion and proliferation

In order to evaluate the possible application of these nanocomposites in the biomedical field, cell viability, proliferation and adhesion were analyzed. On the one hand, short-term cytotoxicity assays were carried out. BC/WBPU5 nanocomposite was chosen for the study since it was the system which presented the best mechanical properties and the highest BC content. Neat BC was also analyzed as reference. The cytotoxicity test results are presented in Fig. 4. a) and b). Fig. 4. a) shows the absorbance versus incubation time for the positive (polyvinyl chloride, PVC) and negative (high density polyethylene, HDPE) controls, as well as for the neat BC and BC/WBPU5. As it can be observed, both BC and BC/WBPU5 nanocomposite displayed nontoxic cell growth, similar to the negative control. The cell proliferation with respect to the negative control as a function of the incubation time is represented in Fig. 4. b). It was observed that the viability of

the L929 cells cultured in the extracted media of both, neat BC and BC/WBPU5 was significantly higher than the established acceptance limit of 70% of this value. Consequently, the obtained results are good indication when thinking on the future biomedical application of the studied polymers.

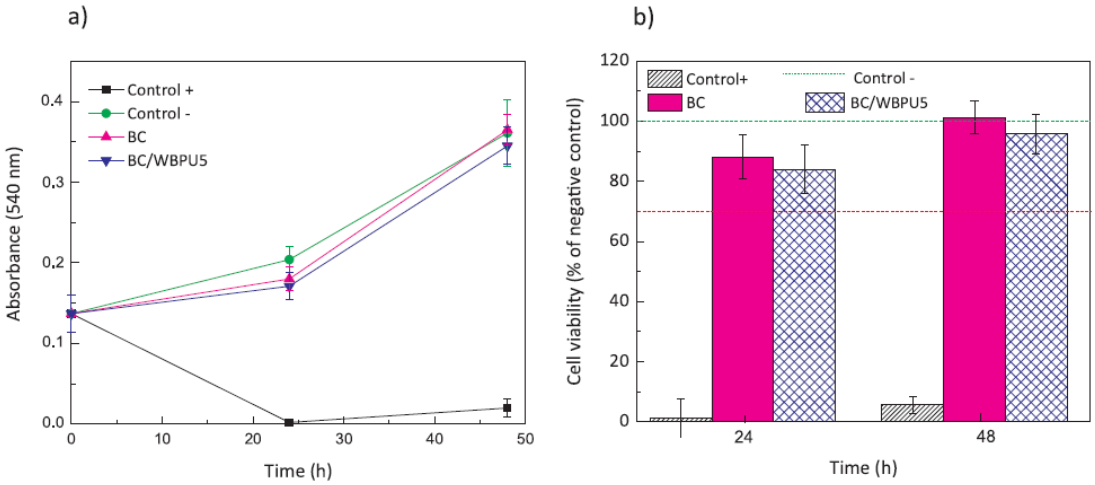

Fig. 4. a) Absorbance at 540 nm versus incubation time of a positive control, negative control, neat BC and BC/WBPU5 and b) Viability of L-929 murine fibroblast cells as function of incubation time.

In addition, long-term cell adhesion test were carried out by Live/Dead assays. Fig. 5 shows the fluorescence confocal microscopy images (x20) where calcein-AM shows cell viability (green) and ethidium homodimer-1 non-viable cells (red). As it can be observed, significant cellular adhesion and proliferation were found for both, neat BC and BC/WBPU5 nanocomposite. There is a large number of adherent cells that show viability (green), and a shortage of dead cells (red). The culture reached the monolayer in 3 days, showing adhesion and stable growth until day 14. In the last stage (C and F), the number of nonviable cells increased, probably due to the high density of the culture. The cells responded in a similar manner to both materials, so since the composition of the materials directly affects cell viability and adhesion, it is concluded that both BC and BC/WBPU nanocomposites are biocompatible materials.

3.3. Shape memory properties

The shape memory properties, namely shape fixity ratio (R_f) and the shape recovery ratio (R_r), of the neat WBPU and two nanocomposites (5 and 120 min of impregnation) are analyzed in this section. The shape recovery process in water as function of time of the neat WBPU and BC/WBPU nanocomposites can be observed in Figure S1 and the results of shape recovery ratio in water along time are shown in Fig. 6. a). All the results are gathered in Table 4.

The shape fixity ratios of the samples summarized in Table 4, suggest that the shape fixity ability is enhanced with the presence of BC. This behavior has been also observed in other works

involving polyurethane matrixes reinforced with nanocellulose and it can be ascribed to the presence of the numerous hydroxyl groups of the BC nano-network (Luo, Hu, & Zhu, 2011; Zhu et al., 2012). These can contribute to the formation of hydrogen bonds between BC and WBPU, resulting in a higher rigidity, increasing the modulus of the material and thus, favouring the fixity of the material´s shape respect to the neat WBPU (Wang, Cheng, Liu, Kang, & Liu, 2018). Moreover, these results are in accordance to the ones obtained by DMA, where it can be seen that the storage modulus of the nanocomposites in the glassy state is higher with the presence of BC respect to the WBPU. According to Ratna and Karger-Kocsis (2008) a high glass state modulus will provide the material with high fixity during simultaneous cooling and unloading.

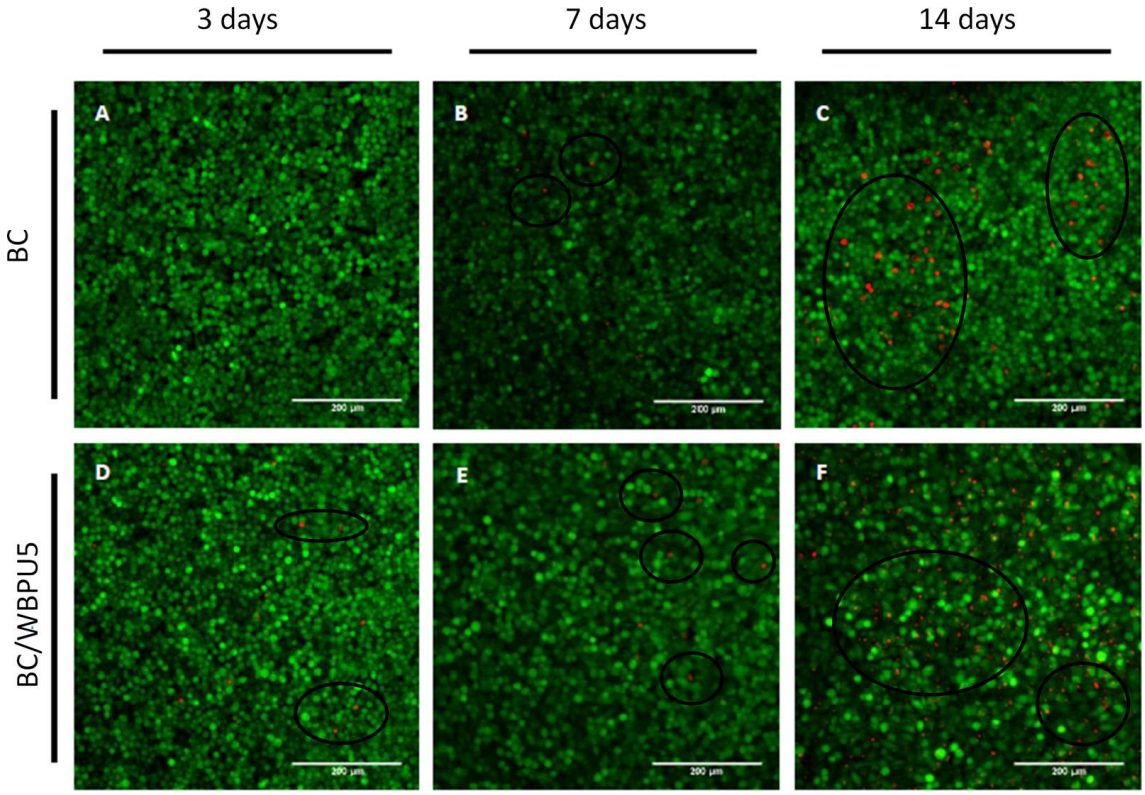

Fig. 5. Adhesion and viability of L929 cells on BC (A–C) and BC/WBPU5 (D–F). Calcein-AM shows cell viability (green) and ethidium homodimer-1 non-viable cells (red/ circles). Images obtained by confocal microscopy (20x) (For interpretation of the references to colour in this figure legend, the reader is referred to the web version of this article).

Considering the possible application of these nanocomposites in medical devices triggered by human body liquids, the shape recovery was analyzed in water at 40 °C. This was set taking into account that the suitable recovery temperature must be slightly higher than body temperature (> 37 °C) but not too high so as not to damage the normal cells and tissues (Cai et al., 2013). As it can be observed in Fig. 6. a), the incorporation of the BC also induces to a faster recovery process due to its hydrophilic nature. The water molecules diffuse through the nanocomposite and the hydrogen bonds between water and BC´s hydroxyl groups make the film become softer, so the

recovery of the original shape is faster (Zhu et al., 2012). In 3 min, the BC/WBPU5 recovered 92.8 ± 6.3% of the original shape, while BC/WBPU120 recovered 72.0 ± 5.1% and neat WBPU only 33.4 ± 9.6%. In the case of the neat WBPU needed 25–30 min to recover 73.0 ± 3.5% of the original shape.

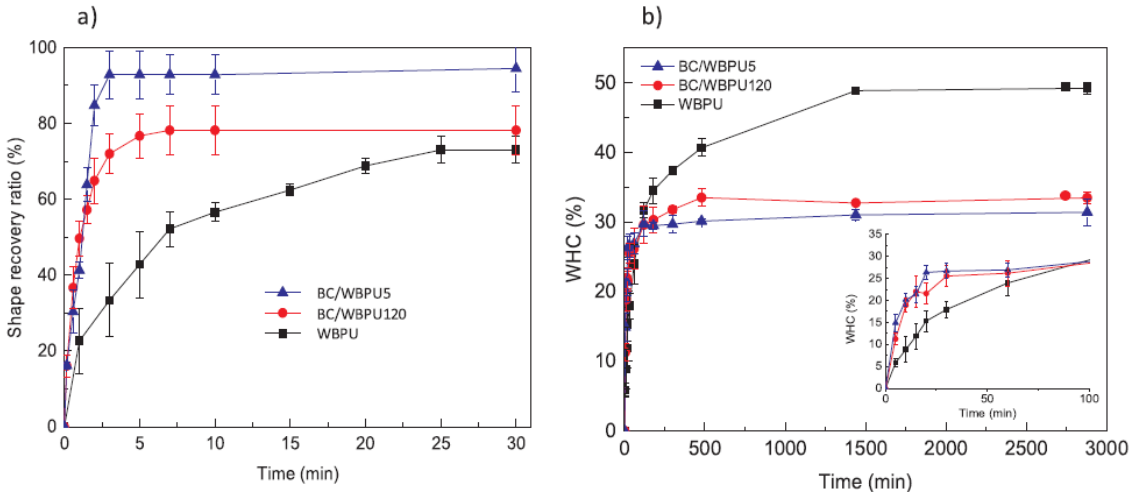

Fig. 6. a) Shape recovery ratio in water and b) WHC of BC/WBPU5 and BC/WBPU120 nanocomposites and neat WBPU (detailed figure corresponds to WHC in the time interval from 0 to 100 min).

Additionally to the presence of BC, the chemical structure and thickness of the nanocomposites as well as the movement of molecular architecture have influence on the shape memory recovery. Huang, Yang, Zhao, & Ding (2010) reported that the recovery ratio in moisture induced recovery is lower than in thermally induced recovery. In moisture induced recovery systems there is a strong dependency on the sample size because the water absorption is easier on the sample´s surface, so the saturation is faster than inside the material. This means that thin films are more suitable for moisture induced recovery systems than bulky materials. In this case, it has been observed (in Table 1) that as impregnation time increased, the thickness of the nanocomposite increased (0.22 ± 0.05 and 0.42 ± 0.05mm for BC/WBPU5 and BC/WBPU120 nanocomposites, respectively) and this can have an influence on the shape memory properties. BC/WBPU5 presented the fastest recovery and was the thinnest nanocomposite, so these results correlated with this fact. Song et al., 2018 also reported that when the material presents a well arrayed layered structure the movement of water molecules in the matrix after immersion in water is favoured. As it has been observed in SEM images (Fig. 1. a), b) and c)), BC presents a layered structure so this fact can help to the recovery process in the nanocomposites. In addition, the temperature at which the test was performed may have helped to the recovery of the shape. As it has been previously reported, the increase of the temperature leads to a weakening of the hydrogen bonding, so the system will have greater recovery capacity (Yildirim, Yurtsever, Yilgor, Yilgor, & Wilkes, 2018). The effect of the temperature can also be important if the recovery temperature is higher than any

transition. As it was observed in the DSC thermograms (Fig. 3. a)), the second transition of the WBPU started around 40 °C, so in this case as the test was performed below the transition temperature, everything indicated that the phenomenon of shape recovery was mainly caused by water and the effect of temperature would be minimal. These results suggest that these materials could be suitable to develop rapid responsive materials for different fields such us sensors, artificial muscles, self-expandable stents or devices involving minimally invasive surgery in the human body.

Table 4. Marginal recovery angle (θ_1), shape fixity (R_f) and recovery (R_r) ratios and maximun water uptake for BC/WBPU5 and BC/WBPU120 nanocomposites, and neat WBPU.

Sample	θ_1 (°)	R_f (%)	R_r (%)$_{3\ min}$	R_r (%)$_{final}$	Maximum water uptake (%)
BC/WBPU5	26.6 ± 4.6	86.0 ± 5.5	92.8 ± 6.3	94.5 ± 7.2	30.1 ± 6.8
BC/WBPU120	32.7 ± 4.7	81.8 ± 2.7	72.0 ± 5.1	78.2 ± 8.4	33.5 ± 6.4
WBPU	43.7 ± 4.8	75.7 ± 2.7	33.4 ± 9.6	73.0 ± 3.5	49.2 ± 0.8

In view of the results of the shape memory test, it was interesting to analyze the water holding capacity (WHC) of neat WBPU and BC/WBPU nanocomposites, since the shape recovery was predictably related to the absorption of water. In order to analyze the influence of the presence of BC in the nanocomposites in the water intake, neat WBPU and BC/WBPU5 and BC/WBPU120 nanocomposites were immersed in water at room temperature for a certain time and the WHC was calculated. It is commonly known that BC presents a high WHC (Azeredo, Barud, Farinas, Vasconcellos, & Claro, 2019; Ul-Islam, Khan, & Park, 2012; Urbina et al., 2017), so the intake of water in the samples was determined and the results are compiled in Fig. 6. b). These results confirmed that water uptake increased rapidly in the presence of BC up to 1 h of immersion. After that moment, BC/WBPU nanocomposites started to approach equilibrium, and after 2 h of immersion the equilibrium was reached. The water uptake of the neat WBPU was slower and the equilibrium was reached between 24 and 48 h of immersion. As it can be observed in Table 4, it can be concluded that the presence of BC induces to a faster water uptake, but limits the water content allowed in the nanocomposite. This could be due to the fact that hydrogen bonding interactions between BC and WBPU (seen in the FTIR study) led to less −OH available in the BC structure to interact with water molecules. This has been also observed by other authors (Popescu, Dogaru, & Popescu, 2017). This can be a positive feature, since absorbed water can accumulate in the interface between components in blends leading to a delamination (Lyu & Untereker, 2009). These results corroborated the ones obtained in the shape memory test since the nanocomposites absorbed more water at shorter times (which would induce a decrease of Tg (Zhang et al., 2018)) and thus, they presented greater recovery and at lower times.

4. CONCLUSIONS

In this work, flexible, transparent and biocompatible nanocomposites with enhanced mechanical performance and water-activated shape memory properties were developed by the combination of BC membranes and WBPU dispersions with potential applications in the biomedical field.

BC wet membranes were immersed in WBPU dispersions for different times and the BC membranes resulted embedded and coated by the WBPU, suggesting the good affinity of both polymers due to their hydrophilic nature. Additionally, the FTIR study revealed hydrogen bond interactions between BC and WBPU. This feature was related to the water holding capacity of the nanocomposites, since the presence of BC limited the water content allowed in the nanocomposite. Mechanical test showed that the elastomeric properties of the WBPU were maintained in the nanocomposites, but an improvement of the modulus and strength of the nanocomposites with respect to the neat WBPU was observed. This suggested the effective BC-reinforcement and it was confirmed by DMA analysis, where it was observed that the storage modulus of the nanocomposites was higher on all temperature range compared to the neat WBPU. The in vitro biocompatibility and cell adhesion tests of the nanocomposites showed non-toxic behaviour making them suitable for biomedical applications. Furthermore, water activated shape memory properties were analyzed by fold-deploy test method. The results revealed an improvement of the shape fixity ability and faster recovery process with the presence of BC. The BC/WBPU5 recovered 92.8 ± 6.3% of the original shape in 3 min, while for the same time period the neat WBPU only 33.4 ± 9.6%. This could be due to the faster diffusion of the water molecules through the nanocomposite and the hydrogen bonding between water and BC hydroxyl groups. The obtained results indicated that 5 min of impregnation time was enough to obtain nanocomposites with improved mechanical performance and fast shape recovery for potential biomedical applications.

Aknowledgements

The authors thank for the financial support from the Spanish Ministry of Economy and Competitiveness (MINECO) (MAT2016-76294-R) and the Basque Government in the frame of Grupos Consolidados (IT-776-13). The authors would also like to acknowledge the technical support provided by SGIker of UPV/EHU. The Basque Government is greatly acknowledged for the PhD grant PIF PRE_2014_1_371 of the researcher Leire Urbina.

References

Alemi, B., & Shodja, H. M. (2018). Effective shear modulus of solids reinforced by randomly oriented- / aligned-elliptic multi-coated nanofibers in micropolar elasticity. Composites Part B Engineering, 143, 197–206. https://doi.org/10.1016/j.compositesb.2018.02.011.

Althouse, G. C., & Hopkins, S. M. (1995). Assesments of boar sperm viability using a combination of two fluorophores. Theriogenology, 43, 595–603. https://doi.org/10.1016/0093-691X(94)00065-3.

Auad, M. L., Contos, V. S., Nutt, S., Aranguren, M. I., & Marcovich, N. E. (2008). Characterization of nanocellulose-reinforced shape memory polyurethanes. Polymer International, 57, 651–659. https://doi.org/10.1002/pi.2394.

Azeredo, H. M. C., Barud, H., Farinas, C. S., Vasconcellos, V. M., & Claro, A. M. (2019). Bacterial cellulose as a raw material for food and food packaging applications. Frontiers in Sustainable Food Systems, 3, 1–14. https://doi.org/10.3389/fsufs.2019.00007.

Bodin, A., Bäckdahl, H., Fink, H., Gustafsson, L., Risberg, B., & Gatenholm, P. (2006). Influence of cultivation conditions on mechanical and morphological properties of bacterial cellulose tubes. Biotechnology and Bioengineering, 97, 425–434. https://doi.org/10.1002/bit.21314.

Cai, Y., Jiang, J.-S., Zheng, B., & Xie, M.-R. (2013). Synthesis and properties of magnetic sensitive shape memory Fe3O4/poly(ε -caprolactone)-Polyurethane Nanocomposites. Journal of Applied Polymer Science, 127, 49–56. https://doi.org/10.1002/app.36849.

Ciolacu, D., Ciolacu, F., & Popa, V. I. (2010). Amorphous cellulose-structure and characterization. Cellulose Chemistry and Technology, 45, 13–21.

El-Fattah, M. A., Hasan, A. M. A., Keshawy, M., El Saeed, A. M., & Aboelenien, O. M. (2018). Nanocrystalline cellulose as an eco-friendly reinforcing additive to polyurethane coating for augmented anticorrosive behaviour. Carbohydrate Polymers, 183, 311–318. https://doi.org/10.1016/j.carbpol.2017.12.084.

Feng, X., Ullah, N., Wang, X., Sun, X., Li, C., Bai, Y., et al. (2015). Characterization of bacterial cellulose by Gluconacetobacter hansenii CGMCC 3917. Journal of Food Science, 80, E2217. https://doi.org/10.1111/1750-3841.13010.

Figueiredo, A. G. P. R., Figueiredo, A. R. P., Alonso-Varona, A., Fernandes, S. C. M., Palomares, T., Rubio-Azpeitia, E., et al. (2013). Biocompatible bacterial cellulosepoly(2-hydroxyethyl methacrylate) nanocomposite films. BioMed Research International, 2013, 1–14. https://doi.org/10.1155/2013/698141.

Guo, L., Sato, H., Hashimoto, T., & Ozaki, Y. (2010). FTIR study on hydrogen-bonding interactions in biodegradable polymer blends of poly(3-hydroxybutyrate) and poly(4-vinylphenol). Macromolecules, 43, 3897–3902. https://doi.org/10.1021/ma100307m.

Hager, M. D., Bode, S., Weber, C., & Schubert, U. S. (2015). Shape memory polymers: Past, present and future developments. Progress in Polymer Science, 3, 49–50. https://doi.org/10.1016/j.progpolymsci.2015.04.002.

Hu, W., Chen, S., Yang, J., Li, Z., & Wang, H. (2014). Functionalized bacterial cellulose derivatives and nanocomposites. Carbohydrate Polymers, 101, 1043–1060. https://doi.org/10.1016/j.carbpol.2013.09.102.

Huang, W. M., Yang, B., Zhao, Y., & Ding, Z. (2010). Thermo-moisture responsive polyurethane shape-memory polymer and composites: A review. Journal of Materials Chemistry, 20, 3367–3381. https://doi.org/10.1039/B922943D.

Jiang, F., Li, T., Li, Y., Zhang, Y., Gong, A., Dai, J., et al. (2018). Wood-based nanotechnologies toward sustainability. Advanced Materials, 30(1703453), 1–39. https://doi.org/10.1002/adma.201703453.

Jiao, L., Xiao, H., Wang, Q., & Sun, J. (2013). Thermal degradation characteristics of rigid polyurethane foam and the volatile products analysis with TG-FTIR-MS. Polymer Degradation and Stability, 98, 2687–2696. https://doi.org/10.1016/j.polymdegradstab.2013.09.032.

Kim, J., Cai, Z., & Chem, Y. (2010). Biocompatible bacterial cellulose composites for biomedical application. Journal of Nanotechnology in Engineering and Medicine, 1, 1–7. https://doi.org/10.1115/1.4000062.

Kiziltas, E. E., Kiziltas, A., & Gardner, D. J. (2015). Synthesis of bacterial cellulose using hot water extracted wood sugars. Carbohydrate Polymers, 124, 131–138. https://doi.org/10.1016/j.carbpol.2015.01.036.

Klemm, D., Schumann, D., Udhardt, U., & Marsch, S. (2001). Bacterial synthesized cellulose-artificial blood vessels for Microsurgery. Progress in Polymer Science, 26, 1561–1603. https://doi.org/10.1016/S0079-6700(01)00021-1.

Liu, Y., Han, C., Tan, H., & Du, X. (2010). Thermal, mechanical and shape memory properties of shape memory epoxy resin. Materials Science and Engineering A, 527, 2510–2514. https://doi.org/10.1016/j.msea.2009.12.014.

Luo, H., Hu, J., & Zhu, Y. (2011). Tunable shape recovery of polymeric nano-composites. Materials Letters, 65, 3583–3585. https://doi.org/10.1016/j.matlet.2011.08.006.

Lyu, S. P., & Untereker, D. (2009). Degradability of polymers for implantable biomedical devices. International Journal of Molecular Sciences, 10, 4033–4065. https://doi.org/10.3390/ijms10094033.

Nakagaito, A. N., Iwamoto, S., & Yano, H. (2005). Bacterial cellulose: The ultimate nanoscalar cellulose morphology for the production of high-strength composites. Applied Physics A, 80, 93–97. https://doi.org/10.1007/s00339-004-2932-3.

Nogi, M., Iwamoto, S., Nakagaito, S. N., & Yano, H. (2009). Optically transparent nanofiber paper. Advanced Materials, 21, 1595–1598. https://doi.org/10.1002/adma.200803174.

Pei, A., Malho, J.-M., Ruokolainen, J., Zhou, Q., & Berglund, L. A. (2011). Strong nanocomposite reinforcement effects in polyurethane elastomer with low volume fraction of cellulose nanocrystals. Macromolecules, 44, 4422–4427. https://doi.org/10.1021/ma200318k.

Picheth, G. F., Pirich, C. L., Sierakowski, M. R., Woehl, M. A., Sakakibara, C. N., Fernandes de Souza, C., et al. (2017). Bacterial cellulose in biomedical applications: A review. International Journal of Biological Macromolecules, 104, 97–106. https://doi.org/10.1016/j.ijbiomac.2017.05.171.

Pinto, E. R. P., Barud, H. S., Silva, R. R., Palmieri, M., Polito, W. L., Calil, V. L., et al. (2015). Transparent composites prepared from bacterial cellulose and castor oil based polyurethane as substrates for flexible OLEDs. Journal of Materials Chemistry C, 3, 11557–11774. https://doi.org/10.1039/c5tc02359a.

Pinto, E. R. P., Barud, H. S., Polito, W. L., Ribeiro, S. J. L., & Messaddeq, Y. (2013). Preparation and characterization of the bacterial cellulose/polyurethane nanocomposites. Journal of Thermal Analysis and Calorimetry, 114, 549–555. https://doi.org/10.1007/s10973-013-3001-y.

Popescu, M.-C., Dogaru, B.-I., & Popescu, C.-M. (2017). The influence of cellulose nanocrystals content on the water sorption properties of bio-based composite films. Materials & Design, 132, 170–177. https://doi.org/10.1016/j.matdes.2017.06.067.

Ratna, D., & Karger-Kocsis, J. (2008). Recent advances in shape memory polymers and composites: A review. Journal of Materials Science, 43, 254–269. https://doi.org/10.1007/s10853-007-2176-7.

Santamaria-Echart, A., Ugarte, L., García-Astrain, C., Arbelaiz, A., Corcuera, M. A., & Eceiza, A. (2016). Cellulose nanocrystals reinforced environmentally-friendly waterborne polyurethane nanocomposites. Carbohydrate Polymers, 151, 1203–1209.

Small, W., Singhal, P., Wilson, T. S., & Maitland, D. J. (2010). Biomedical applications of thermally activated shape memory polymers. Journal of Materials Chemistry, 20, 3356–3366. https://doi.org/10.1016/j.carbpol.2016.06.069.

Solanki, A., Das, M., & Thakore, S. (2018). A review on carbohydrate embedded polyurethanes: An emerging area in the scope of biomedical applications. Carbohydrate Polymers, 181, 1003–1016. https://doi.org/10.1016/j.carbpol.2017.11.049.

Song, L., Li, Y., Xiong, Z., Pan, L., Luo, Q., Xu, X., et al. (2018). Water-Induced shape memory effect of nanocellulose papers from sisal cellulose nanofibers with graphene oxide. Carboydrate Polymers, 179, 110–117. https://doi.org/10.1016/j.carbpol.2017.09.078.

Sun, W., & Huang, M. (2010). Thermo/moisture responsive shape-memory polymer for possible surgery/operation inside living cells in future. Materials & Design, 31, 2684–2689. https://doi.org/10.1016/j.matdes.2009.11.036.

Thomas, B., Raj, M. C., Athira, K. B., Rubiyah, M. H., Joy, J., Moores, A., et al. (2018). Nanocellulose, a versatile green platform: From biosources to materials and their applications. Chemical Reviews, 118, 11575–11625. https://doi.org/10.1021/acs.chemrev.7b00627.

Ul-Islam, M., Khan, T., & Park, J. K. (2012). Water holding and release properties of bacterial cellulose obtained by in situ and ex situ modification. Carbohydrate Polymers, 88, 596–603. https://doi.org/10.1016/j.carbpol.2012.01.006.

Urbina, L., Algar, I., García-Astrain, C., Gabilondo, N., González, A., Corcuera, M. A., et al. (2016). Biodegradable composites with improved barrier properties and transparency from the impregnation of PLA to bacterial cellulose membranes. Journal of Applied Polymer Science, 24(5), 2071–52082. https://doi.org/10.1002/app.43669.

Urbina, L., Hernández-Arriaga, A. M., Eceiza, A., Gabilondo, N., Corcuera, M. A., Prieto, M. A., et al. (2017). By-products of the cider production: An alternative source of nutrients to produce bacterial cellulose. Cellulose, 24, 2071–2082. https://doi.org/10.1007/s10570-017-1263-4.

Wan, T., & Chen, D. (2018). Mechanical enhancement of self-healing waterborne polyurethane by graphene oxide. Progress in Organic Coatings, 121, 73–79. https://doi.org/10.1016/j.porgcoat.2018.04.016.

Wang, Y., Cheng, Z., Liu, Z., Kang, H., & Liu, Y. (2018). Cellulose nanofibers/polyurethane shape memory composites with fast water-responsivity. Journal of Materials Chemisitry B, 6, 1668–1677. https://doi.org/10.1039/c7tb03069j.

Wang, X., Zhang, Y., Liang, H., Zhou, X., Fang, C., Zhang, C., et al. (2019). Synthesis and properties of castor oil-based waterborne polyurethane/sodium alginate composites with tunable properties. Carbohydrate Polymers, 208, 391–397. https://doi.org/10.1016/j.carbpol.2018.12.090.

Wu, J., Zheng, Y., Song, W., Luan, J., Wen, X., Wu, Z., et al. (2014). In situ synthesis of silver-nanoparticles/bacterial cellulose composites for slow-released antimicrobial wound dressing. Carbohydrate Polymers, 102, 762–771. https://doi.org/10.1016/j.carbpol.2013.10.093.

Wu, G.-M., Liu, G-f., Chen, J., & Kong, Z-w. (2017). Preparation and properties of thermoset composite films from two-component waterborne polyurethane with low loading level nanofibrillated cellulose. Progress in Organic Coatings, 106, 170–176. https://doi.org/10.1016/j.porgcoat.2016.10.031.

Yildirim, E., Yurtsever, M., Yilgor, E., Yilgor, I., & Wilkes, G. L. (2018). Temperature dependent changes in the hydrogen bonded hard segment network and microphase morphology in a model polyurethane: Experimental and simulation studies. Journal of polymer science, part B: Polymers physics, 56, 182–192. https://doi.org/10.1002/polb.24532.

Zhang, Z-x., Qi, X-d., Li, S-t., Yang, J-h., Zhang, N., Huang, T., et al. (2018). Water actuated shape-memory and mechanically-adaptive poly(ethylene vinyl acetate) achieved by adding hydrophilic poly (vinyl alcohol). European Polymer Journal, 98, 237–245. https://doi.org/10.1016/j.eurpolymj.2017.11.031.

Zhang, P., Xu, P., Fan, H., Sun, Z., & Wen, J. (2019). Covalently functionalized graphene towards molecular-level dispersed waterborne polyurethane nanocomposite with balanced comprehensive performance. Applied Surface Science, 471, 595–606. https://doi.org/10.1016/j.apsusc.2018.11.235.

Zhou, X., Li, Y., Fang, C., Li, S., Cheng, Y., Lei, W., et al. (2015). Recent advances in synthesis of waterborne polyurethane and their application in water-based ink: A review. Journal of Materials Science & Technology, 31, 708–722. https://doi.org/10.1016/j.jmst.2015.03.002.

Zhu, Y., Hu, J., Luo, H., Young, R. J., Deng, L., Zhang, S., et al. (2012). Rapidly switchable water-sensitive shape-memory cellulose/elastomer nano-composites. Soft Matter, 8, 2509–2517. https://doi.org/10.1039/c2sm07035a.